Structures of a Ag monolayer deposited on Cu(111), Cu(100), and Cu(110) substrates: An extended tight-binding quenched-molecular-dynamics study

C. Mottet* and G. Tréglia*
Laboratoire de Physique des Solides, Bâtiment 510, Centre Universitaire de Paris–Sud, 91405 Orsay CEDEX, France

B. Legrand
DTM/Section de Recherches de Métallurgie Physique, Centre d'Etudes Nucléaires de Saclay, 91191 Gif-sur-Yvette CEDEX, France

(Received 20 April 1992)

We determine the atomic structure of a Ag monolayer deposited on the three low-index faces of a Cu substrate by means of an extended tight-binding quenched-molecular-dynamics simulation. For the (111) face, the most stable structure is a $p(10\times10)$ one. The surface plane is strongly waving, the perturbation extending up to the first ten surface layers. For the (100) face, the pseudohexagonal reconstruction $c(10\times2)$ is stablized with respect to pseudomorphy and pseudoepitaxy. The case of the (110) face is more intricate. As a function of the Ag coverage, we predict a sequence of superstructures going from the $p(2\times7)$ missing-row reconstruction at low coverage up to the pseudohexagonal $p(7\times2)$ reconstruction at the monolayer completion.

I. INTRODUCTION

The metallic multilayers give rise to an increasing interest due to their magnetic and catalytic properties.[1] These properties are strongly dependent on the regularity of the artificial multilayer structures, which is driven by the topological and chemical nature of the interface between the various components. Hence, it is of prime importance to understand the atomic structure of the first deposited monolayer. Let us note that a very similar problem arises in the case of very strong surface segregation in very dilute alloys. Our aim here is to model this phenomenon in the particular case of one Ag monolayer either deposited on a Cu substrate or obtained by segregation in a very dilute Cu(Ag) alloy,[2,3] for which experimental data can be found for the three low-index faces: (111),[3–12] (100),[3,13–15] and (110).[3,16]

Let us recall that the growth mode of an A metal onto a B substrate is usually classified according to three types.[17,18] When there is no wetting, one observes island formation (Volmer-Weber) whereas a complete wetting corresponds to a layer-by-layer growth (Frank–van der Merwe). An intermediate case is the incomplete wetting, i.e., a layer-by-layer growth followed by island formation (Stranski-Krastanov). From the macroscopic point of view, it is possible to predict the growth mode according to the so-called *wetting* energy,[19,20]

$$S_{A/B}=\gamma_A+\gamma_{AB}-\gamma_B\ , \tag{1}$$

where γ_i is the surface energy of the i metal and γ_{AB} is the interface energy. Thus, A wets the B substrate when $S_{A/B}<0$. This criterion simplifies in the case of bimetallic systems for which the difference in surface energy is large compared to the interface term (which is generally small). This is indeed the case for the Ag-Cu system since $\gamma_{Ag}\ll\gamma_{Cu}$,[21] so that $S_{Ag/Cu}<0$. The Ag growth on a Cu substrate is then of the layer-by-layer type, the remaining question being, what is the atomic structure of the Ag plane at the completion of the first monolayer? Three kinds of superstructures can be considered:[20] *pseudomorphy,* where the deposited A atoms occupy the positions of the underlying B lattice (which occurs when the deposit-substrate *interlayer* interactions prevail over the deposit-deposit *lateral* ones); *pseudoepitaxy,* in which the deposited atoms form a layer which presents the same crystallographic structure than the B substrate, but keep adatom-adatom distances along the close-packed rows as near as possible as those of the pure A metal (which happens for strong deposit-deposit *lateral* interactions); and *reconstruction* which, at least for the open faces, allows (when the deposit-deposit interactions are very strong) a compacting of the surface compared to pseudoepitaxy. For instance, in the case of the square (100) and rectangular (110) orientations, the deposit can prefer a pseudohexagonal structure.

In practice, except for pseudomorphy, the deposited atoms occupy inequivalent sites with respect to the substrate lattice. As a consequence, assuming a rigid bidimensional adlayer is far from being realistic, it is then important to relax the structure in order to determine the most stable equilibrium position. Therefore, it is necessary to model the interatomic forces in the framework of a potential which satisfactorily accounts for such relaxations. This requires the use of *N-body potentials* derived from the electronic structure, since it is known that the usual empirical *pair potentials* are unable to reproduce the inward relaxation of the pure metal surfaces.[22,23] Once such a potential is granted, all the inequivalent atoms have to be individually relaxed, which is only possible within numerical procedures such as the quenched molecular dynamics, which will be used here.

The present paper is then organized as follows. First, in Sec. II, we will briefly describe the numerical simula-

tion techniques and the interatomic potentials we use. Then, in Sec. III, we will discuss the peculiar problems which arise when comparing superstructures with different periodicities and patterns. In Sec. IV, we will present our results concerning the equilibrium structures of an Ag monolayer on top of the three low-index faces [Sec. IV A, (111); Sec. IV B, (100), and Sec. IV C, (110)] of a Cu substrate. Finally, a comparison between the different orientations will be given with a conclusion in Sec. V.

II. THEORETICAL MODEL

Let us summarize the principles of extended tight-binding quenched molecular dynamics (TBQMD). The relaxation procedure consists of integrating the equation of motion,

$$F_i(t)=m_i\frac{dv_i(t)}{dt}\ , \tag{2}$$

where $v_i(t)$ is the velocity at time t of atom i of mass m_i, and $F_i(t)$ is the force acting on this atom at this time.[24] The quenching procedure, in which v_i is canceled when the product $F_i(t)v_i(t)$ is negative, leads to the minimization of the potential energy at 0 K.[25] The force is calculated in the extended tight-binding formalism from the total energy,[26]

$$E_i=E_i^r+E_i^b\ , \tag{3}$$

where E_i^r is a repulsive energy given by[27]

$$E_i^r=\sum_{j,r_{ij}<r_c}A_{IJ}\exp\left[-p_{IJ}\left[\frac{r_{ij}}{r_{IJ}^0}-1\right]\right]\ . \tag{4}$$

K $(=I,J)$ denotes the chemical nature of atom k, r_{II}^0 is the first-neighbor distance of pure metal I, and $r_{IJ}^0=(r_{II}^0+r_{JJ}^0)/2$ if $J\neq I$, r_{ij} is the distance between atoms i and j, and r_c is the cutoff distance for the interaction.

E_i^b is the band energy obtained from the *extended* tight-binding Hamiltonian[28]

$$H=\sum_{i\neq j}|i\rangle\beta_{ij}^{IJ}\langle j|+\sum_i|i\rangle\epsilon_i^I\langle i|\ , \tag{5}$$

where β_{ij}^{IJ} are hopping integrals with

$$\beta_{ij}^{IJ}=\beta_0^{IJ}\exp\left[-q_{IJ}\left[\frac{r_{ij}}{r_{IJ}^0}-1\right]\right] \tag{6}$$

and the on-site term ϵ_i^I depends on the local environment[28,29]

$$\epsilon_i^I=\alpha_I\left[\sum_{i\neq j}(\beta_{ij}^{IJ})^2\right]^{1/2}\ . \tag{7}$$

From Eqs. (5)–(7), taking into account charge-neutrality requirements,[30,31] one obtains the band energy term for a *full d* band,

$$E_i^b=-\left\{\sum_{j,r_{ij}<r_c}\bar{\beta}_{IJ}^2\exp\left[-2q_{IJ}\left[\frac{r_{ij}}{r_{IJ}^0}-1\right]\right]\right\}^{1/2}\ , \tag{8}$$

with

$$\bar{\beta}_{IJ}=10\alpha_I\beta_0^{IJ}\ . \tag{9}$$

The parameters $(A_{IJ},p_{IJ},q_{IJ},\bar{\beta}_{IJ})$ are fitted to the experimental values of the cohesive energy, lattice parameter, and elastic constants for the pure metals $(J=I)$. For the cross terms $(J\neq I)$, A_{IJ} and $\bar{\beta}_{IJ}$ are obtained from the dissolution energies of one impurity of A into B and vice versa. p_{IJ} and q_{IJ} are the arithmetic averages of the pure metal values. More details on this derivation are given in Appendix A together with the numerical values in the particular case of the Cu-Ag system. The presence of the square root in Eq. (8) is at the origin of the correct description of surface relaxations.[22,23] The force on atom i is then obtained from

$$F_i=-\frac{dE_{\rm tot}}{dr_i}\ , \tag{10}$$

with

$$E_{\rm tot}=\sum_i E_i\ . \tag{11}$$

Using Eqs. (3), (4), and (8), one then obtains the expression of the force acting on atom i,

$$\mathbf{F}_i=\sum_{j,r_{ij}\ll r_c}F_{ij}\frac{\mathbf{r}_{ij}}{r_{ij}} \tag{12}$$

with

$$F_{ij}=-2A_{IJ}\frac{p_{IJ}}{r_{IJ}^0}\exp\left[-p_{IJ}\left[\frac{r_{ij}}{r_{IJ}^0}-1\right]\right]-\left[\frac{1}{E_i^b}+\frac{1}{E_j^b}\right]\frac{q_{IJ}}{r_{IJ}^0}\exp\left[-2q_{IJ}\left[\frac{r_{ij}}{r_{IJ}^0}-1\right]\right]\bar{\beta}_{IJ}^2\ . \tag{13}$$

An interesting microscopic quantity in a system containing a high number of inequivalent sites is the local pressure defined at $T=0$ K by[32,33]

$$P_i=-\frac{dE_i}{d\ln V}\ , \tag{14}$$

where V is the atomic volume. The sign of P_i gives the stress sign:positive for a compression and negative for a tension. Using Eqs. (3), (4), and (8), one gets

$$P_i=\tfrac{1}{3}\sum_{j,r_{ij}<r_c}A_{IJ}\frac{r_{ij}}{r_{IJ}^0}\exp\left[-p_{IJ}\left[\frac{r_{ij}}{r_{IJ}^0}-1\right]\right]-\frac{\bar{\beta}_{IJ}^2}{E_i^b}q_{IJ}\frac{r_{ij}}{r_{IJ}^0}\exp\left[-2q_{IJ}\left[\frac{r_{ij}}{r_{IJ}^0}-1\right]\right]\ . \tag{15}$$

III. COMPARISON BETWEEN SUPERSTRUCTURES: PECULIAR SIMULATION PROBLEMS

Our goal is to compare the relative stabilities of the different possible superstructures for an Ag adlayer over a Cu substrate by means of numerical simulation. In

practice, this sets the problem of replacing the infinite crystal by a finite box subject to periodic-boundary conditions along directions parallel to the surface. In the perpendicular direction, we do not use such periodic conditions, which implies working with a thin film, sufficiently thick to recover bulk properties in the midlayer.[34] It it worth noticing that the choice of the periodic-boundary conditions forces the periodicity of the superstructure to be equal to (or at least a divisor of) the two-dimensional (2D) box size. Obviously, this procedure is unable to account for incommensurate superstructures; only their simplest approximants can be described. From a local point of view, both structures are very similar and should lead to differences in energy which are beyond the accuracy of our calculations. Furthermore, for a given periodicity, we have to optimize the pattern and in particular the number of Ag atoms in the mesh. In the present case, we systematically use as initial conditions the pseudomorphy, the pseudoepitaxy, and various possible reconstructions.

From a practical point of view, we then have to compare boxes with different sizes (to simulate different periodicities). Moreover, for a given periodicity, the number of atoms being fixed *a priori* during the simulation, we have to check different initial fillings of the mesh. Another way to proceed is to overfill the initial pattern and to allow the elimination of the atoms which spontaneously tend to rise up into adatom positions by the size-mismach-induced limited ejections, (SMILE) mechanism.[35,36] This requires us to define a critical height beyond which the Ag atom is taken off the simulation box. In our calculations, this critical height is allowed to vary between $d/2$ and d, where d is the interlayer distance.

Once the various superstructures are optimized via the relaxation algorithm, one defines the most stable one as the structure which presents the minimum adsorbtion energy per Ag atom[37] $E_{\rm ads}(\theta)$,

$$E_{\rm ads}(\theta)=\frac{E_{\rm tot}(\theta)-E_{\rm tot}(\theta=0)}{N_{\rm Ag}}-\mu_{\rm Ag}\ , \tag{16}$$

where θ is the Ag absolute coverage, defined as

$$\theta=\frac{N_{\rm Ag}}{N_{\rm Cu}}\ , \tag{17}$$

$N_{\rm Ag}$ and $N_{\rm Cu}$ being the numbers of Ag and Cu atoms in the 2D mesh of the superstructure. $E_{\rm tot}(\theta)$ is the total energy (11) of the slab with a θ coverage and $\mu_{\rm Ag}$ is the chemical potential of the Ag vapor phase. Note that $E_{\rm tot}(\theta=0)$ corresponds with the initial pure Cu slab with its two free surfaces and that knowledge of the numerical value of $\mu_{\rm Ag}$ is not required here since $\mu_{\rm Ag}$ disappears when comparing two different superstructures. In practice, we will set $\mu_{\rm Ag}=0$. Finally, note that other definitions of the coverage could have been chosen, as can be seen in Appendix B.

IV. SUPERSTRUCTURES OF AN Ag MONOLAYER ON TOP OF A Cu SUBSTRATE

A. Ag/Cu(111)

As explained above, we will successively study the pseudomorphy, the pseudoepitaxy, and a contractive reconstruction similar to that observed in Au(111). A constant guide for the choice of the numerical cell is the geometrical criterion, which allows us to accommodate the size mismatch along the closed-packed ⟨110⟩ directions. This leads to use boxes which contain n Cu atoms and $n_{\rm Ag}=n+\delta n$ Ag atoms along ⟨110⟩ with

$$n=\frac{\delta n}{r^*-1}\ , \tag{18}$$

where r^* is the ratio of Cu to Ag atomic radii

$$r^*=\frac{r^0_{\rm Cu}}{r^0_{\rm Ag}}=0.886\ . \tag{19}$$

The simplest solution of (18) is obtained for $\delta n=-1$, which gives $8<n=8.75<9$. Note that a better agreement should be achieved for higher values of δn (for example, -4, -9, etc.) which leads indeed to very large cells but, once more, to local configurations not really different from those obtained for $\delta n=-1$. In practice, we will use, in the following, boxes containing around nine Cu atoms along the ⟨110⟩ direction.

1. Pseudomorphy

Even though this is not necessary in this simple case, we take a (9×9) box along [1-10] and [10-1] in order to allow a relaxation satisfying the above-mentioned geometrical criterion [Eqs. (18) and (19)]. The first time, we perform the TBQMD simulation starting from an initial pseudomorphic condition at $T=0$ K. In such a case, due to the symmetry of the system adsorbate substrate, only vertical displacements are possible. Thus a spontaneous evolution towards the pseudoepitaxy or a reconstruction is forbidden. The main result is the rather high value of the adsorption energy,

$$E_{\rm ads}(\theta=1)=-2.625\ \text{eV/atom}\ .$$

The corresponding value of the p-plane relaxation ($p=0$: surface, etc.) is given by

$$d^*_p=\frac{d_{p,p+1}-d^0_{p,p+1}}{d^0_{p,p+1}}\ , \tag{20}$$

where $d_{p,p+1}$ is the (average) relaxed interlayer distance between the planes p and $p+1$, and $d^0_{p,p+1}$ is the corresponding unrelaxed distance, which is taken equal to the pure interlayer spacing for $p>0$, and to the average of this spacing in Ag and Cu pure metals for $p=0$. One finds

$$d^*_0=+4.3\,\%,\quad d^*_1=-0.2\,\%\ .$$

It is possible to break the symmetry of the pseudomorphy by heating the initial configuration. Starting from an ini-

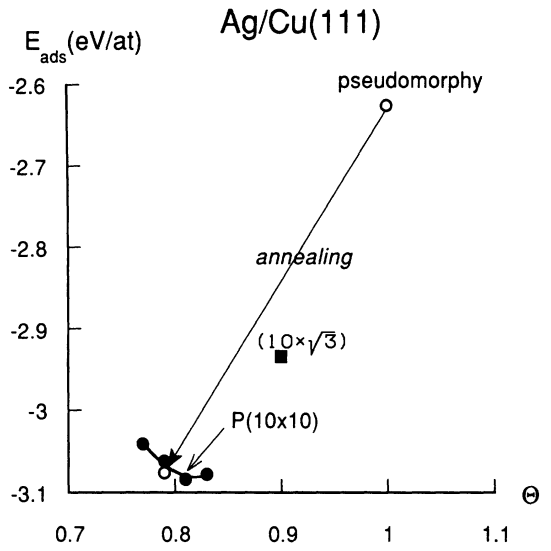

FIG. 1. Variation of the adsorption energy E_{ads} with the absolute coverage θ for the Ag/Cu(111) system. Full dots denote pseudoepitaxy ($n \times n$), open dots denote pseudomorphy (the arrow indicates the effect of the annealing procedure), and the full square denotes Au(111)-type reconstruction ($10 \times \sqrt{3}$).

tial temperature of $T = 500$ K, the SMILE effect occurs, leading to the ejections of about two crossed close-packed rows and to a strong lowering of the adsorption energy which becomes (see Fig. 1)

$$E_{ads}(\theta = 0.79) = -3.076 \text{ eV/atom} .$$

The corresponding density of the Ag overlayer is very close to the pure Ag(111) one (see Appendix B). This means that a pseudoepitaxial structure around the geometrical criterion is favored. One has then to optimize this kind of superstructure, which is the object of the next section.

2. *Pseudoepitaxy* ($n \times n$)

In order to optimize the periodicity of such a superstructure, we start from various ($n \times n$) initial pseudoepitaxial structures with n varying aroud the geometrical criterion ($n \cong 9$). The adsorption energy curve is plotted in Fig. 1. One sees that the minimum value of $E_{ads}(\theta)$ is obtained for $n = 10$,

$$E_{ads}(\theta = 0.81) = -3.080 \text{ eV/atom} ,$$

the minimum being rather flat between $n = 10$ and 11. The corresponding coverage $\theta = 0.81$ is slightly higher than the coverage of an ideal Ag(111) overlayer ($\theta = 0.785$, see Appendix B). The average relaxations are

$$d_0^* = +1.6\%, \quad d_1^* = -1.2\% .$$

This pseudoepitaxy implies that all the Ag atoms sit in inequivalent sites, going from ternary sites (of both the hcp and fcc type) to top sites, through various intermediate positions (bridge, etc.). One then expects some corru-

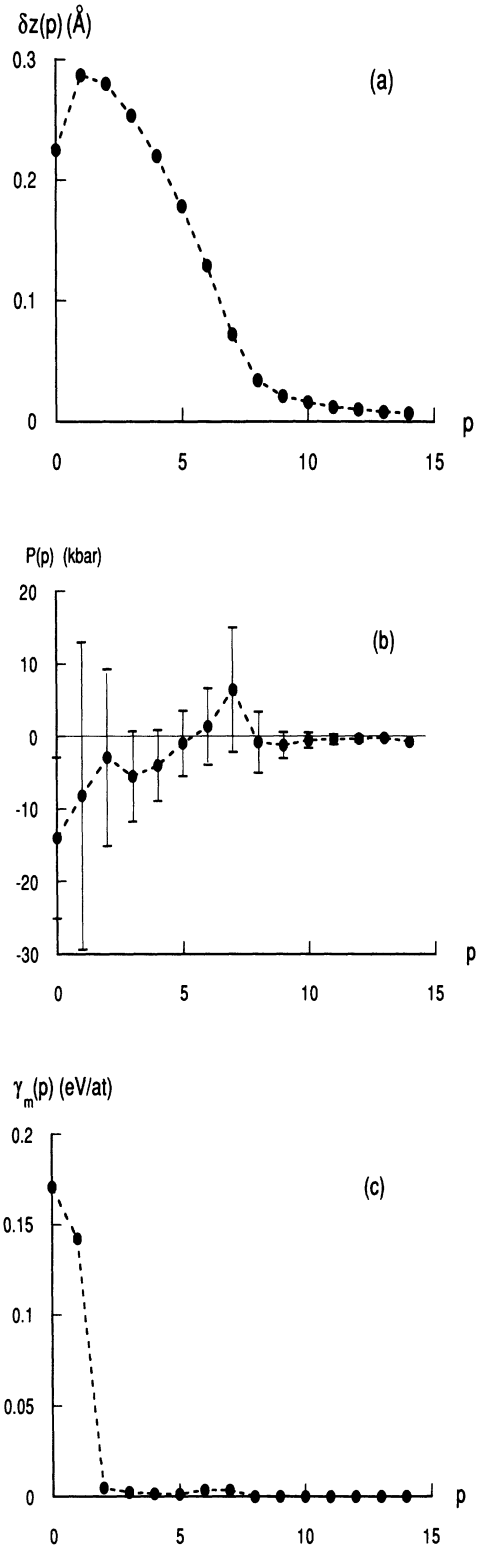

FIG. 2. Depth profile ($p = 0$, Ag adlayer; $p = 1$, first Cu layer, etc.), for the Ag/Cu(111) system, of (a) the corrugation $\delta z(p)$ [average thickness defined in (21)] of the p layer; (b) the average pressure of the p-layer $P(p)$ (the bars indicate the mean-square amplitude of the corresponding distribution of local pressures); and (c) the p-layer tension $\gamma_m(p)$ [average energy defined in (23)].

gation of the Ag layer. A measure of the corrugation of the p layer is given by its average thickness

$$\delta z(p)=\left[\frac{1}{N_p}\sum_{i=1}^{N_p}[z_i-z_m(p)]^2\right]^{1/2}, \tag{21}$$

where $z_m(p)$ is the average elevation of the p plane

$$z_m(p)=\frac{1}{N_p}\sum_{i=1}^{N_p} z_i \ . \tag{22}$$

N_p is the number of atoms in the p plane and z_i is the elevation of the atom i. The p dependence of $\delta z(p)$ is shown in Fig. 2(a). The surface Ag plane is found to be strongly corrugated [$\delta z(0)=0.23$ Å], the maximum amplitude between the lowest and highest atoms reaching 1 Å, i.e., one-half of the interlayer spacing $d_{0,1}=2.22$ Å. More surprisingly, as can be seen in Fig. 2(a), this corrugation is very important in the first five layers and then damped to become negligible beyond the fifteenth layer. A perspective view of this superstructure is given in Fig. 3(a), illustrating this corrugation and its extension into the substrate. As can be seen, the surface layers are undulating, presenting hills and hollows, which correspond to hcp and on-top positions, respectively, contrary to the common idea. Furthermore, the elevation of the fcc sites is less important than the hcp ones. In Fig. 4, we see that the expansion of the Ag plane relative to the Cu substrate along the close-packed directions is rather uniform, the Ag atoms not being locked in the fcc or hcp positions. A good correlation is obtained for the Ag plane between the local pressure defined in (15) and the elevation: the deeper the Ag atom is, the more negative (tension) the local pressure is. Conversely, the Ag atoms in hcp position have a positive (compression) local pressure. This observation is modified for the first Cu planes: the atoms of the first five planes which are in the propagated hollow are in compression and not in tension (see Fig. 5). It is interesting to remark that the profile of the layer energies defined as

$$\gamma_m(p)=\frac{1}{N_p}\sum_{i=1}^{N_p}[E_i-E_{\rm coh}({\rm Cu})] \ , \tag{23}$$

is more rapidly damped [Fig. 2(c)] than the pressure [Fig. 2(b)] and corrugation [Fig. 2(a)] profiles. It can be understood if one realizes that the local environments, beyond the second layer, are not so different from those of bulk atoms, even at the bottom of the hollows.

The present results show the necessity of taking into account the multilayer character of the superstructure, which was not the case in general up to now. A fixed substrate treatment should have missed in the present case the corrugation of the top layer and obviously of the selvedge, as can be seen in Fig. 3(b).

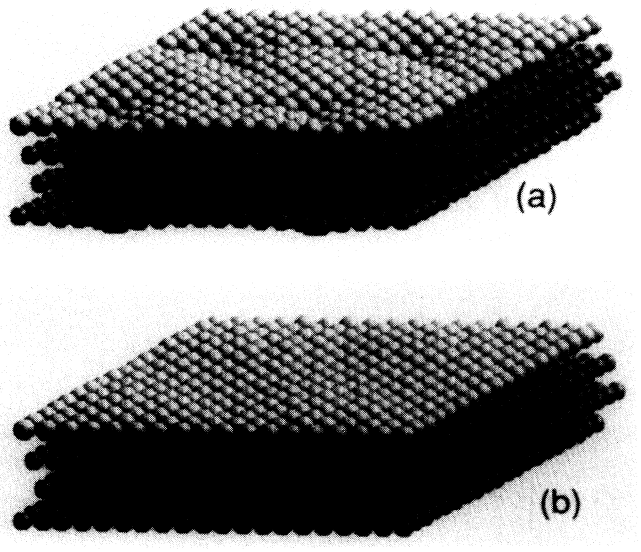

FIG. 3. Perspective view of the Ag/Cu(111) $p(10\times10)$ superstructure. Four unit cells are shown. For the sake of clarity, the scale of the z axis has been magnified by a factor of 2. The white spheres indicate the Ag atoms and the black spheres denote those of the Cu substrate: (a) fully relaxed structure (mobile substrate), (b) approximation of a rigid substrate.

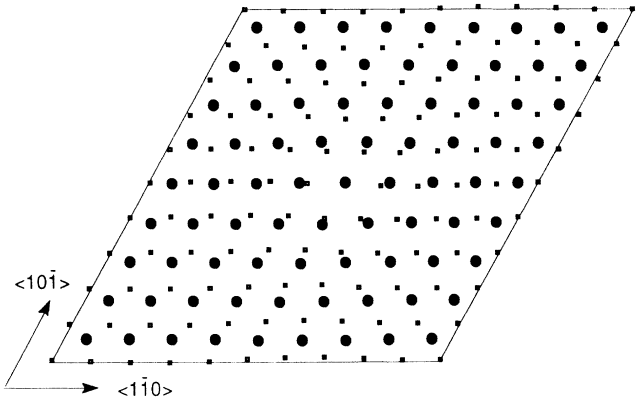

FIG. 4. Top view of the unit cell of the Ag/Cu(111) $p(10\times10)$ superstructure: the full dots indicate the Ag atoms of the adlayer and the squares indicate the atoms of the first layer of the Cu substrate.

3. *Reconstruction of the Au(111) type*

One can ask whether a more stable structure could be obtained from the analogy with the reconstruction observed in the pure Au(111) surface.[38–48] Let us recall that this reconstruction, which is attributed to the pure surface tensile strain, allows the surface layer to get a more close-packed structure than the (111) plane. The main difference with the previous $p(10\times10)$ 2D pseudoepitaxy has to be found in its uniaxial character which leads to a 1D pseudomorphy along the [11-2] direction and to a 1D pseudoepitaxy along the [1-10] direction. The relaxed $(10\times\sqrt{3})$ superstructure presents almost no corrugation [$\delta z(0)=0.07$ Å] and, as can be seen in Fig. 1, its adsorption energy

$$E_{\rm ads}(\theta=0.9)=-2.934 \text{ eV/atom}$$

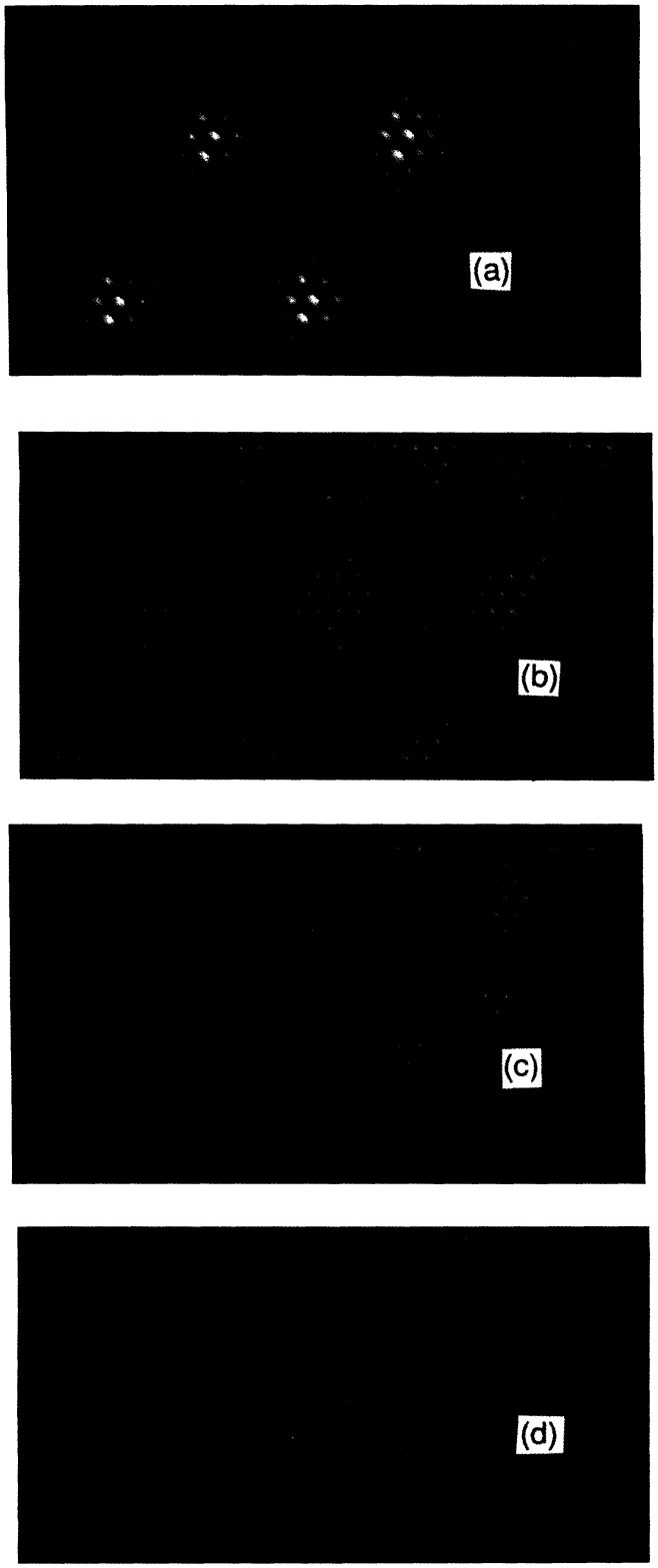

FIG. 5. Pressure map of the first four planes for the Ag/Cu(111) $p(10\times10)$ structure for the four cells shown in Fig. 3. (a) Ag adlayer, (b) Cu first underlayer, (c) Cu second underlayer, and (d) Cu third underlayer. The gray scale illustrates the pressure variation from the most tensile sites (white spheres, $P_{\min}=-135$ kbar) up to the most compressed ones (black spheres, $P_{\max}=94$ kbar).

lies between the pseudomorphy and the definitively stablest $p(10\times10)$ pseudoepitaxy.

4. Comparison with experiments

Our main conclusion for Ag/Cu(111) is the stability of the corrugated $p(10\times10)$ superstructure. This periodicity compares fairly well to experiments which suggest a $(9\pm1\times9\pm1)$ one.[3,4] To our knowledge, there is no observation of the precise atomic pattern. We hope that the present study will stimulate scanning tunneling microscopy, Rutherford backscattering spectroscopy, or quantitative low-energy electron diffraction studies to probe the existence of the unexpected corrugation revealed in the present work.

B. Ag/Cu(001)

1. Pseudomorphy

As for the (111) face, the symmetry of the pseudomorphic adsorbate-substrate system forbids any lateral displacement at $T=0$ K. Thus, we only obtain a vertical relaxation

$$d_0^*=+7.5\,\%,\quad d_1^*=-0.1\,\%$$

and a high value of the adsorption energy

$$E_{\rm ads}(\theta=1)=-2.871\ \text{eV/atom}\ .$$

In order to break the symmetry of the pseudomorphy, we anneal the initial structure, starting from a (10×10) box to account for the geometrical criterion. Once again, the SMILE effect leads to about 12 ejections, corresponding to $\theta=0.88$. As can be seen in Fig. 6, the adsorption energy is significantly decreased,

$$E_{\rm ads}(\theta=0.88)=-3.047\ \text{eV/atom}\ .$$

A close inspection of the surface structure resulting from these ejections reveals a strong tendency to form hexagons, obtained through a shift of every second [1-10] row along the [1-10] direction. In particular, this rearrangement leads to a shorter periodicity in the perpendicular [110] direction so that the final superstructure is closely related to a $c(10\times2)$ periodicity. This pseudohexagonal reconstruction presents a strong analogy with the one encountered in the $5d$ pure metals (Ir,Pt,Au).[39,49–56] In view of the irregularity of the Ag hexagons, we now try to optimize the structure by starting from pseudohexagonal reconstructions $(n\times2)$ for various values of n around the geometrical criterion ($n=9$).

2. Pseudohexagonal reconstruction $(n\times2)$

In order to be consistent with the interaction range of the potential, we use $(n\times4)$ boxes with $7<n<14$. As can be seen in Fig. 6, the minimum of the adsorption energy is very flat around $n=10$–11,

$$E_{\rm ads}(\theta=0.90)=-3.066\ \text{eV/atom}\ .$$

Moreover, one checks that the actual periodicity of the superstructure is indeed $(n\times2)$ so that the simulation

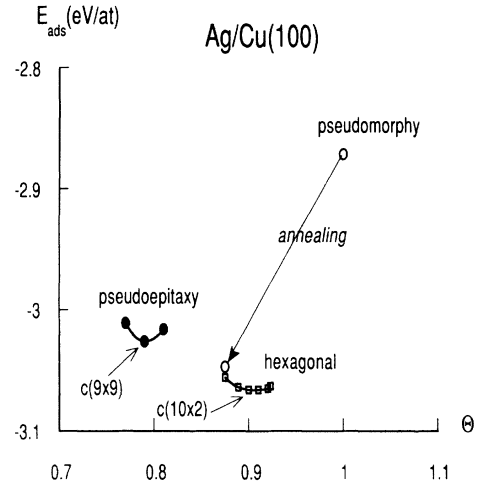

FIG. 6. Variation of the adsorption energy E_{ads} with the absolute coverage θ for the Ag/Cu(100) system. Full dots denote pseudoepitaxy ($n \times n$), open dots denote pseudomorphy (the arrow indicates the effect of the annealing procedure), and open squares denote hexagonal reconstruction ($n \times 2$).

boxes contain two elementary cells. This is in very good agreement with the experimental data which conclude with a $c(10\times2)$ superstructure. For this $c(10\times2)$ periodicity, the Ag atoms form a quasiregular hexagonal lattice, with a slight dilation of about 4% $[1-5/(3\sqrt{3})]$ in the [110] direction and a rather large outwards relaxation ($d_0^* = +11.2\%$). It is then tempting to check up on the relative stability of the regular hexagonal structure, which then corresponds to a (10×25) perodicity ($\theta=0.935$), with respect to the (10×2) one ($\theta=0.900$). The simulation performed on a (10×25) box sets the SMILE effect in action, leading to eight ejections and $\theta=0.904$, i.e., a coverage very close to an ideal Ag(111) plane (see Appendix B). The corresponding value of the adsorption energy,

$$E_{ads}(\theta=0.904) = -3.059 \text{ eV/atom} ,$$

is slightly higher, meaning that the $c(10\times2)$ is the most stable structure. The registry of an hexagonal layer on a square substrate implies the existence of many in equivalent sites, and then a corrugation of the adlayer. One can then wonder to what extent this corrugation can be compared to the spectacular one previously shown in the case of a hexagonal-hexagonal deposit (Sec. IV A 2). One sees in Fig. 7 that this is not the case: the adlayer is remarkably flat [$\delta z(0)=0.08$ Å], the maximum amplitude being 0.2 Å. As a consequence, contrary to the previous (111) case, one observes no perturbation of the Cu substrate.

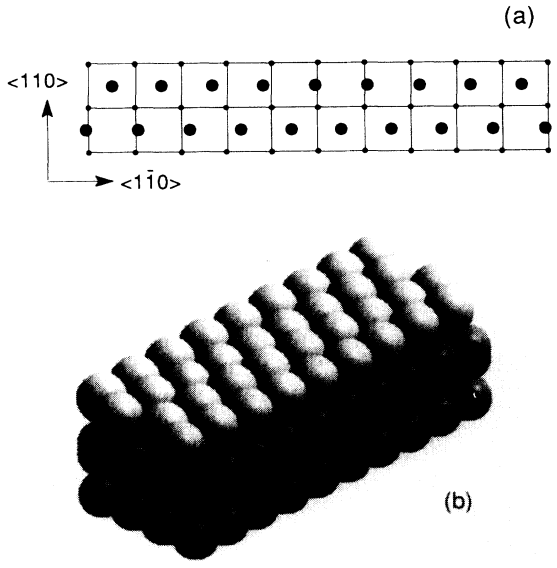

FIG. 7. $c(10\times2)$ Ag/Cu(100) pseudohexagonal structure. (a) Top view (one unit cell): the large dots denote the Ag adatoms, and the small dots denote the Cu atoms of the first underlayer. (b) Perspective view (two unit cells): the white spheres indicate the Ag adatoms and the black spheres denote the Cu substrate atoms. For the sake of clarity, the scale of the z axis has been magnified by a factor of 2.

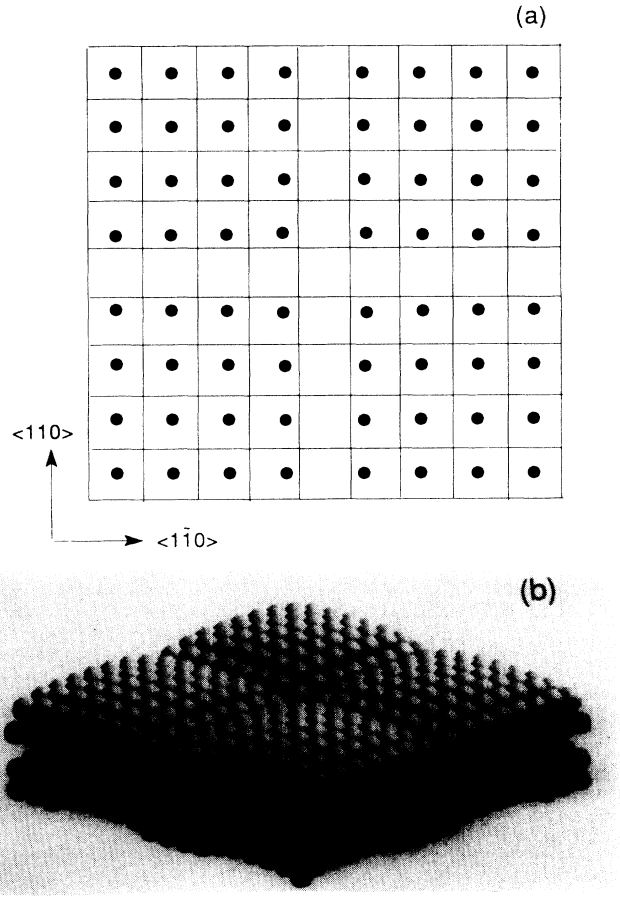

FIG. 8. $c(9\times9)$ Ag/Cu(100) pseudoepitaxial structure. (a) Top view (one unit cell): the large dots denote the Ag adatoms, and the small dots denote the Cu atoms of the first underlayer. (b) Perspective view (four unit cells): the white spheres indicate the Ag adatoms and the black spheres indicate the Cu substrate atoms. For the sake of clarity, the scale of the z axis has been magnified by a factor of 2.

3. *Pseudoepitaxy* ($n \times n$)

Even though the annealing procedure clearly leads to a pseudohexagonal-type reconstruction of the Ag layer, one can wonder about its stability compared to the third kind of superstructure quoted in the Introduction: a pseudoepitaxy ($n \times n$) for n values around the geometrical criterion ($n \cong 9$). As can be seen in Fig. 6, this group of superstructures appears for lower values of θ ($\theta \cong 0.8$). The minimum of the adsorbtion energy, which now is reached for the value of the geometrical criterion,

$$E_{\text{ads}}(\theta=0.79)=-3.026 \text{ eV/atom} ,$$

is found well above the value for the $c(10\times2)$ superstructure. This pseudoepitaxy occurs with a strong corrugation extending deep into the substrate (about 10 layers) as in the (111) case. This is illustrated in Fig. 8(b). A major difference is that now the misfit is accommodated through localized dislocations [Fig. 8(a)] instead of extended ones. These dislocations border domes with square bases of eight Ag atom sides. This superstructure preserves the fourfold symmetry of the substrate, which reduces the number of inequivalent sites and then confers a regular shape on it. This strongly differs from the $p(10\times10)$ Ag/Cu(111) superstructure where the threefold symmetry is lost, leading to a more irregular structure.

4. *Discussion and comparison with experiments*

To summarize our results for Ag/Cu(001), we have optimized two kinds of superstructures corresponding to different coverage ranges: the $c(9\times9)$ pseudoepitaxy ($\theta \cong 0.8$) and the $c(10\times2)$ pseudohexagonal reconstruction ($\theta \cong 0.9$), the latter one having the lowest adsorption energy. This is in complete agreement with the experimental observation of the $c(10\times2)$ superstructure at the completion of the first monolayer.[3,6,14] However, one can wonder about the possible occurrence of the $c(9\times9)$ structure for lower coverages. Up to now, experiments have not shown the stability of this structure. This can be understood from Fig. 6, which is characteristic of *attractive interactions* between adsorbates (at least up to $\theta \cong 0.9$), the most close-packed structure being the most stable one. This means that, even for low coverages, the Ag layer structure is made of $c(10\times2)$ islands which grow with increasing θ. It is worth noting that this $c(10\times2)$ Ag/Cu(001) superstructure (hexagonal adlayer on a square substrate) is significantly less corrugated than the $p(10\times10)$ Ag/Cu(111) one (hexagonal adlayer on an hexagonal substrate). The topology of this pseudohexagonal reconstruction is very similar to that observed for the (001) surface of pure 5*d* metals, even though we have not optimized here the rotational angle of the hexagonal lattice with respect to the square substrate.[51,57] In particular, the corrugation found here (0.2 Å between the lowest and highest atoms) compares fairly well with the value obtained for the pure metals (0.5 Å),[50] the difference being consistent with the larger value of the outwards relaxation obtained in the present heteroatomic case (11% compared to 3%).

C. Ag/Cu(110)

The (110) surface is the most open low-index face. Its rectangular primitive cell exhibits two inequivalent directions: one ([1-10]) is close packed and the other ([001]) is open. Therefore, the variety of possible atomic rearrangements is larger than for the other orientations. Furthermore, let us recall that the (110) face of the 5*d* transition metals (Ir,Pt,Au) undergoes the well-known *missing-row* reconstruction[58–71] which, instead of compacting the surface, has the reverse effect. Even though neither Cu or Ag undergo this reconstruction as pure metals, one can wonder if it could occur for the Ag/Cu(110) system. In the following, we will then optimize successively the pseudomorphy, the pseudoepitaxy, and then two types of reconstruction: a contractive pseudohexagonal one [by analogy with the (001) face] and the missing-row one [by analogy with the (110) faces of 5*d* metals].

1. *Pseudomorphy*

As for the other two orientations, the numerical simulation of an unannealed pseudomorphy only leads to vertical displacements due to the symmetry of the Ag/Cu(110) system,

$$d_0^* = 11.9\%, \quad d_1^* = -3.4\% .$$

The corresponding value of the adsorption energy is noticeably lower than for the other orientations,

$$E_{\text{ads}}(\theta=1)=-3.037 \text{ eV/atom} .$$

The annealing of this pseudomorphy keeps the structure unchanged, indicating no preference for any ordered superstructure. Let us note that this annealing leads to large-amplitude (and low-frequency) vibrations along the [001] direction, as already mentioned for the pure Cu(110) surface.[72] The quenching procedure can then set some problems for this orientation by freezing these vibrational states. To avoid it, we will replace the annealing by starting from various initial configurations at $T=0$ K, beginning with the pseudoepitaxy.

2. *Pseudoepitaxy* $p(1\times n)$

The geometrical criterion in the [1-10] direction leads again to a periodicity $n=9$ along it. In the less close-packed [001] direction, it is reasonable to think that the pseudomorphy is preferred, leading to $p(1\times n)$ pseudoepitaxy. As can be seen in Fig. 9, the minimum is reached for $n=8$,

$$E_{\text{ads}}(\theta=0.875)=-3.092 \text{ eV/atom} ,$$

which is lower than the pseudomorphy, the difference being significantly smaller than for the other two orientations. The corresponding structure, illustrated in Fig. 10(a), does not exhibit a so-pronounced corrugation [$\delta z(0)=0.08$ Å] as for the (111) and (001) pseudoepitaxies but instead a strong oscillatory relaxation,

$$d_0^* = 18.8\%, \quad d_1^* = -5.0\% .$$

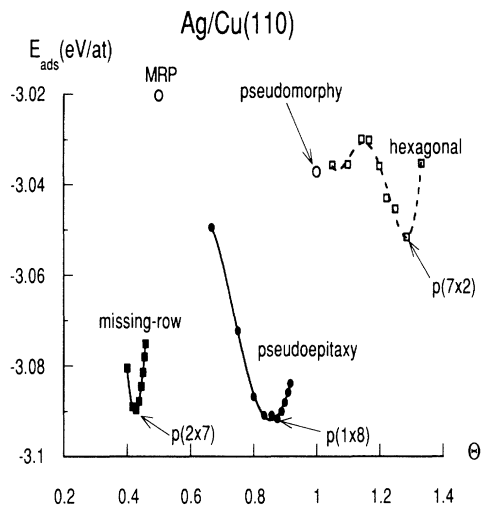

FIG. 9. Variation of the adsorption energy E_{ads} with the absolute coverage θ for the Ag/Cu(110) system. Full squares denote missing-row reconstruction $(2\times n)$, full dots denote pseudoepitaxy $(1\times n)$, open dots denote pseudomorphy and MRP, and open squares denote hexagonal reconstruction $(n\times 2)$.

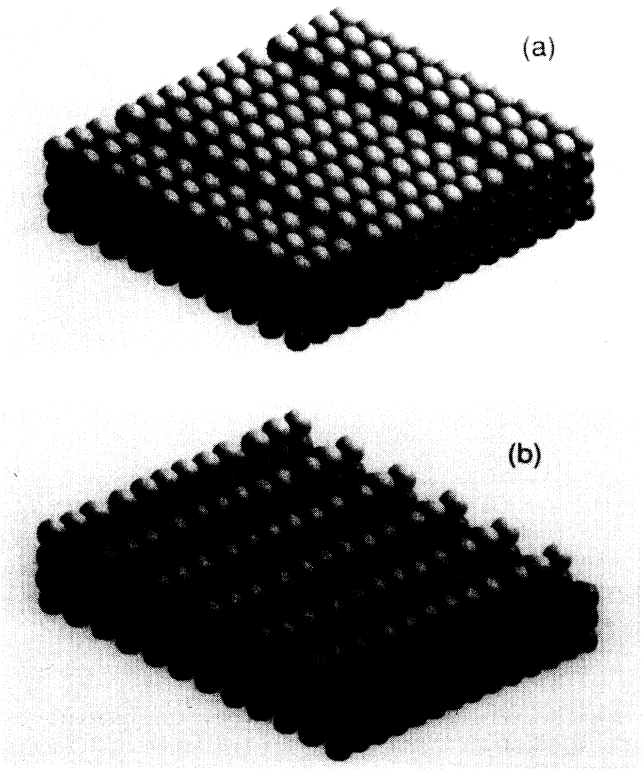

FIG. 10. Perspective view of the Ag/Cu(110) $p(1\times 8)$ [(a) pseudoepitaxy, 18 unit cells] and $p(2\times 7)$ [(b) missing-row reconstruction, 12 unit cells] superstructures. The white spheres indicate the Ag atoms and the black spheres indicate those of the Cu substrate.

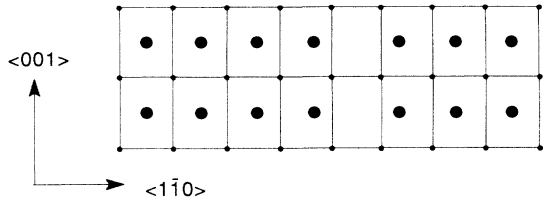

FIG. 11. Top view of two unit cells of the Ag/Cu(110) $p(1\times 8)$ superstructure. The large dots indicate the Ag atoms of the adlayer and the small dots indicate the Cu atoms of the first underlayer.

Let us remark that, as for the $c(9\times 9)$ Ag/Cu(001) pseudoepitaxy, but contrary to the $p(10\times 10)$ Ag/Cu(111) one and to the $c(10\times 2)$ Ag/Cu (001) reconstruction, the misfit is accommodated through an array of localized edge dislocations with a Burgers vector $\mathbf{b}=a/2$ [1-10]. The atomic structure of the Ag layer can then be analyzed in terms of chains, seven atoms long, lying in the [1-10] channels, separated by a pseudovacancy (see Fig. 11).

3. *Pseudohexagonal reconstruction* $(n\times 2)$

As for the (001) orientation, it is possible to compact the Ag layer by forming hexagons in which the Ag close-packed rows lie now along the open [001] direction, every second row being shifted along this direction. In that case, the geometrical criterion (18) has to be rewritten along the open $\langle 001\rangle$ direction, which gives (see Appendix B),

$$n=\frac{\delta n}{r^*\sqrt{2}-1}=\frac{\delta n}{0.2526}\ . \tag{24}$$

At the difference of the (001) and (111) cases, the compacting of the surface is achieved now by adding Ag atoms along this direction, the simplest cells being obtained for $\delta n=1$ $(n=4)$ and $\delta n=2$ $(n=8)$. We have then optimized the adsorption energy with respect to n for these two values of δn. As can be seen in Fig. 9, the minimum is obtained for the $p(7\times 2)$ structure, i.e., $\delta n=2$ and $n=7$. The corresponding relaxed pseudohexagonal structure is shown in Fig. 12. The corrugation on the first plane [$\delta z(0)=0.29$ Å] is found to be more important than for the near-hexagonal $c(10\times 2)$ superstructure on the (100) face and even more than for the (111) face. This corrugation is accompanied by a very large dilation contraction of the first interlayer distances,

$$d_0^*=53.9\%,\quad d_1^*=-7.9\%\ .$$

Surprisingly, its adsorption energy

$$E_{ads}(\theta=1.286)=-3.052\ \text{eV/atom}$$

is found well above that of the $p(1\times 8)$ pseudoepitaxy and even hardly lower than that of the pseudomorphy (see Fig. 9), although it corresponds to a higher coverage $(\theta=1.286)$. The origin of this unusual behavior has to be

related to the probable repulsive character of the effective interactions between [1-10] Ag chains, as has been found for the pure Au(110) surface or for Cu or Ag(110) under stress.[70,71]

4. *Missing-row reconstruction $p(2\times n)$*

If repulsive effective interactions really exist between [1-10] Ag chains, one can expect a great stability of a missing-row-type reconstruction.[70,71] As for the pseudoepitaxy, we have to optimize the periodicity n along the [1-10] direction, whereas every second [1-10] Ag chain is missing. The minimum of the adsorption energy is now obtained for $n=7$ (see Fig. 9),

$$E_{\rm ads}(\theta=0.43)=-3.090 \text{ eV/atom} .$$

This value is very close to that found for the $p(1\times 8)$ pseudoepitaxy and significantly lower than for the $p(7\times 2)$ pseudohexagonal reconstruction, which confirms the repulsive character (or at lest the weakness) of the effective interactions between [1-10] Ag chains. The $p(2\times 7)$ superstructure, illustrated in Fig. 10(b), has the same characteristics as the $p(1\times 8)$ pseudoepitaxy, i.e., the misfit is accomodated by an array of pseudovacancies, separating Ag chains, now six atoms long. The corresponding relaxations are lower than for the pseudoepitaxy,

$$d_0^*=9.7\%, \quad d_1^*=-3.1\% .$$

One can note in Fig. 9 that, similarly to what is observed when going from pseudomorphy to pseudoepitaxy (1×8), the adsorption energy of the $p(2\times 7)$ structure is significantly lower than the missing-row pseudomorphy (MRP) $p(2\times 1)$.

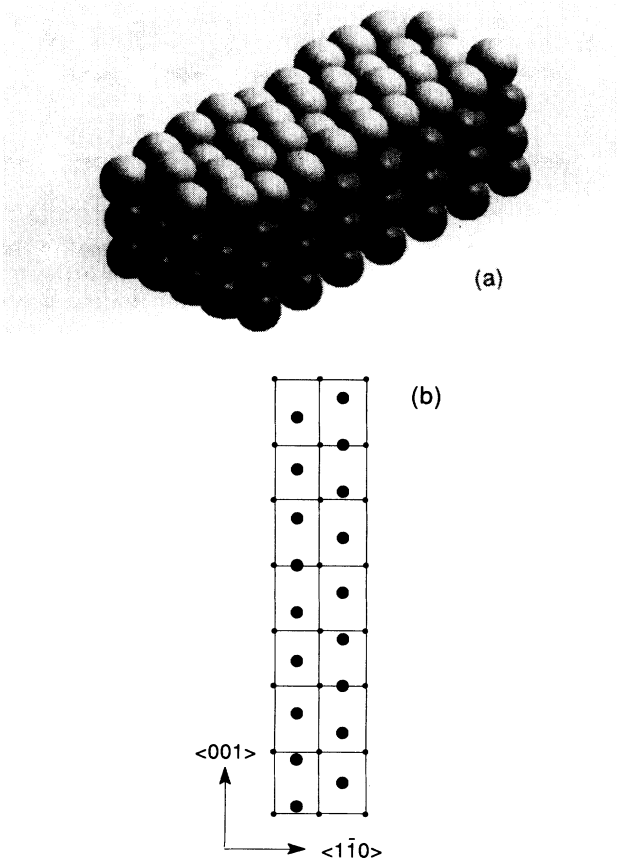

FIG. 12. $p(7\times 2)$ Ag/Cu(110) pseudohexagonal structure. (a) Perspective view (two unit cells). The white spheres indicate the Ag adatoms and the black spheres indicate the Cu substrate atoms. (b) Top view (one unit cell). The large dots denote the Ag adatoms, and the small dots indicate the Cu atoms of the first underlayer.

5. *Discussion and comparison with experiments*

The great variety of experimental results indicates the peculiarity of the (110) surface.[3,16] Whereas, for the (111) and the (100) faces, only the $(9\pm 1\times 9\pm 1)$ pseudoepitaxy and the $c(10\times 2)$ pseudohexagonal reconstruction are observed, a large number of superstructures are mentioned as a function of the coverage for the (110) face:[3,16] a $p(1\times 8)$ or a $p(1\times 5)$, depending on the temperature for $\theta<0.9$ and a $p(7\times 2)$ or a $c(4\times 2)$ for $\theta\cong 1.25$. Moreover, some indications for the occurrence of another structure at $\theta\cong 0.5$ are also given, consistent with the missing-row reconstruction.[16] Thus a very rich phase diagram (θ,T) is suspected for the (110) face, as expected in the presence of attractive effective interactions between Ag adatoms along the [1-10] direction and repulsive ones perpendicular to this direction.[70,71] This is in good agreement with our simulations, which give only the stable structures at $T=0$ K.

V. CONCLUSION

Using the extended tight-binding quenched-molecular-dynamics simulation, we have determined the atomic structures of an Ag monolayer deposited on the three low-index faces (111), (100), and (110) of a Cu substrate.

On the (111) and the (100) faces, we have obtained near-hexagonal monolayer structures. A very unexpected result is the multilayer corrugation found for the (111) face: the Ag atoms, which are on top positions, embed themself in the substrate, instead of rising up above the surface. This leads to a strong corrugation, which affects the first 10 layers of the substrate. This result shows the severe limitation of the often-made rigid substrate approximation. A consequence of this extended corrugation can occur in the superficial segregation phenomenon.[35,36] As mentioned in Sec. IV A 2, due to the undulations, some sites in the selvedge are in compression: it means that they would be preferentially occupied by small atoms. This suggests a decoration method to obtain a local pressure map near the surface.[33]

This study points out a major difference between the "isotropic" (111) and (100) faces and the more anisotropic (110) one. For the first two orientations, the deposited layer has a tendency to compact itself up to (or even slightly above) the pure close-packed Ag(111) plane density, similarly to pure $5d$ metal surfaces: Au(111) reconstruction with a compacting of about 4%,[40,45,48] and Ir, Pt, and Au (100) reconstructions with the formation of

TABLE I. Parameters values for Ag and Cu.

	A (eV)	p	$\bar{\beta}$ (eV)	q	B (eV/atom)	C_{44} (eV/atom)	C' (eV/atom)	E_{coh} (eV/atom)	r^0 (Å)
Cu	0.0894	10.55	1.2799	2.43	10.44	5.74	1.91	−3.50	2.56
					(10.44)	(6.03)	(1.91)	(−3.50)	(2.56)
Ag	0.1031	10.85	1.1895	3.18	11.55	5.35	1.92	−2.95	2.89
					(11.55)	(5.45)	(1.82)	(−2.95)	(2.89)

distorted hexagons.[49–56] This has to be related to the tensile strain found for the unreconstructed metal surfaces.[73] On the other hand, very open superstructures are stabilized for the (110) surface. In other words, the interactions between Ag adsorbates are attractive for the (111) and (100) orientations, as is generally admitted for a metal-metal system, but repulsive (at least between adjacent close-packed rows) for the (110) face.

Finally, let us mention the various modes adopted to accommodate the size mismatch along the close-packed [110] directions: the accommodation is homogeneous for the near-hexagonal superstructures whereas we observe an array of very localized dislocations for cubic or rectangular structures.[74–79] The latter situation can better be described in terms of pseudovacancies which can be disordered at $T\neq 0$ K.[80–85] It should then be tempting to rationalize these differences by means of a Frenkel-Kontorowa–type[86] model, while keeping in mind that the rigid substrate approximation inherent to this model may be too severe. Current work is under progress in this direction.

ACKNOWLEDGMENTS

It is a great pleasure to thank B. Aufray and J. Eugéne for having pointed out to us the peculiar behavior of the Ag/Cu system and for fruitful discussions. I. Shteto is greatly acknowledged for enlightening comments on the SMILE effect.

APPENDIX A: DERIVATION OF THE INTERATOMIC POTENTIALS FOR THE Cu-Ag SYSTEM

The parameters $(A,p,q,\bar{\beta})$ defined in Eqs. (4) (6), and (9) are fitted, for the pure metals, to the experimental values of the cohesive energy E_{coh}, the lattice parameter a, the bulk modulus B, and the elastic constants C_{44} and C',[87]

$$E_{coh}=6A(2+R_2)-\bar{\beta}\sqrt{6(2+E_2)}\ , \tag{A1}$$

$$\left.\frac{\partial E_{coh}}{\partial r}\right|_a=0\Longrightarrow 6pA(2+R_2\sqrt{2})=\bar{\beta}q\frac{(12+6E_2\sqrt{2})}{(12+6E_2)^{1/2}}\ , \tag{A2}$$

$$B=\frac{4Ap^2}{3}(1+R_2)-\frac{\sqrt{2}q^2\bar{\beta}}{9(6+3E_2)^{3/2}}\times[(6+3E_2\sqrt{2})^2+36E_2(1-\sqrt{2})^2]\ , \tag{A3}$$

$$C_{44}=pA(p-1-R_2\sqrt{2})-\frac{q\bar{\beta}}{(12+6E_2)^{1/2}}(2q-1-E_2\sqrt{2})\ , \tag{A4}$$

$$C'=\frac{pA}{2}(p-3+4pR_2)-\frac{q\bar{\beta}}{(12+6E_2)^{1/2}}(q-\tfrac{3}{2}+4qE_2)\ , \tag{A5}$$

with $E_2=\exp[-2q(\sqrt{2}-1)]$ and $R_2=\exp[-p(\sqrt{2}-1)]$.

In these formulas, the repulsive interactions and the hopping integrals are extended up to the next-nearest neighbors. They are linked up to zero with a fifth-order polynomial to avoid discontinuities both in the energy and in the forces. To ensure that the homoatomic interactions do not change when going from the pure metal to the alloy, we use this polynomial termination from the biggest distance between next-nearest neighbors (here the Ag one) up to the smallest distance between third neighbors (here the Cu one). The values of the parameters $(A,p,q,\bar{\beta})$ for both metals are given in Table I, with a comparison between the experimental[88,89] and the calculated values of E_c, a, B, C_{44}, and C'. The agreement is very satisfactory.

The heteroatomic terms $(A_{IJ},p_{IJ},q_{IJ},\bar{\beta}_{IJ})$ are obtained from the heat of dissolution of one impurity of Ag in Cu and vice versa. Due to the importance of the size effect between Cu and Ag, it is of prime importance to allow the atoms to relax to obtain these energies. We then adopt a trial-and-error method to get A_{IJ} and $\bar{\beta}_{IJ}$, p_{IJ} and q_{IJ} being given by an arithmetic average of the pure

TABLE II. Heteroatomic parameters with heats of solution ΔH.

	A (eV)	p	$\bar{\beta}$ (eV)	q	ΔH (Cu in Ag) (eV/atom)	ΔH (Ag in Cu) (eV/atom)
Cu-Ag	0.0977	10.70	1.2275	2.805	0.276	0.396

metal parameters. The values of the heteroatomic parameters are given in Table II with the heats of solution ΔH (A in B) and ΔH (B in A) used in the fitting procedure.[90] As for the pure metals, we impose the heteroatomic interaction to go to zero at the same distance by a fifth-order polynomial.

APPENDIX B: COVERAGES AND DENSITIES OF THE SUPERSTRUCTURES

We present here the correspondence between the absolute atomic surface density (in atoms/cm^2) and the various possible definitions for the coverage, either as the ratio θ between the numbers of Ag and Cu atoms in the 2D mesh [absolute coverage defined in Eq. (17)] or expressed in Ag(111) monolayer (ML) units θ_{ML}. This is illustrated in Table III in the case of all the most stable superstructures determined for the three low-index orientations.

One observes that the superstructures obtained "at the completion" for the three low-index faces correspond in each case to θ_{ML} close to unity. This can suggest a new criterion for the choice of the optimal periodicity, which differs, except for the (111) face, from the geometrical one developed in the main text [Eqs. (18), (19), and (24)]. Namely, $\theta_{ML}=1$ leads to the following: for the pseudoepitaxy of the (111) face, $n=\delta n/(r^*-1)$; for the hexagonal reconstruction of the (100) face, $n=\sqrt{3}\delta n/[2(r^*)^2-\sqrt{3}]$ and for the hexagonal reconstruction of the (110) face, $n=\sqrt{3}\delta n/[\sqrt{8}(r^*)^2-\sqrt{3}]$.

For the last structure, it is interesting to note that this criterion leads to n very close to an integer value ($n=7$) for $\delta n=2$, in good agreement with the observation of the $p(7\times2)$ superstructure.

TABLE III. Surface densities and coverages for the three low index orientations.

Face	Superstructure	Density (10^{15} atoms/cm^2)	$\theta=\frac{N_{Ag}}{N_{Cu}}$ [Eq. (17)]	θ_{ML}
(111)	pure Ag	1.383	0.785	1.000
	$p(10\times10)$	1.427	0.810	1.032
	Pseudomorphy	1.762	1.000	1.274
(100)	pure Ag	1.197	0.785	0.866
	$c(9\times9)$	1.206	0.790	0.872
	$c(10\times2)$	1.373	0.900	0.993
	Pseudomorphy	1.526	1.000	1.103
(110)	$p(2\times7)$	0.463	0.429	0.335
	pure Ag	0.847	0.785	0.612
	$p(1\times8)$	0.944	0.875	0.683
	Pseudomorphy	1.079	1.000	0.780
	$p(7\times2)$	1.388	1.286	1.003

*Present address: CRMC2, Centre National de la Recherche Scientifique, Campus de Luminy, Case 913, 13288 Marseille CEDEX 9, France.

[1]See, for intance, *Multilayers Synthesis, Properties and Nonelectronic Applications,* edited by T. W. Barbee, F. Spaepen, and L. Greer, MRS Symposia Proceedings No. 103 (Materials Research Society, Pittsburgh, 1988).
[2]Y. Liu and P. Wynblatt, Surf. Sci. **240**, 245 (1990); **241**, L21 (1991).
[3]J. Eugène, thesis, Marseille, 1989; J. Eugène, B. Aufray, and F. Cabané, Surf. Sci. **241**, 1 (1991).
[4]K. A. R. Mitchell, D. P. Woodruff, and G. W. Vernon, Surf. Sci. **46**, 418 (1974).
[5]Y. Namba and R. W. Vook, Thin Solid Films **82**, 165 (1981).
[6]E. Bauer, Surf. Sci. **7**, 351 (1967).
[7]E. Bauer, Appl. Surf. Sci. **11/12**, 479 (1982).
[8]M. J. Gibson and P. J. Dobson, J. Phys. F **5**, 1828 (1975).
[9]A. P. Shapiro, A. L. Wachs, and T. C. Chiang, Solid State Commun. **58**, 12 (1986).
[10]Y. Borensztein, Europhys. Lett. **4**, 723 (1987); Y. Borensztein, T. Lopez-Rios, and G. Vuye, Phys. Rev. B **37**, 6235 (1988).
[11]A. P. Shapiro, T. C. Hsieh, A. L. Wachs, T. Miller, and T. C. Chiang, Phys. Rev. B **38**, 7394 (1988).
[12]P. A. Huttunen and A. Vehanen, Phys. Rev. B **42**, 11 570 (1990).
[13]P. W. Palmberg and T. N. Rhodin, J. Chem. Phys. **49**, 147 (1968).
[14]J. G. Tobin, S. W. Robey, and D. A. Shirley, Phys. Rev. B **33**, 2270 (1986); J. G. Tobin, S. W. Robey, L. E. Klebanoff, and D. A. Shirley, *ibid.* **35**, 9056 (1987).
[15]J. E. Black, D. L. Mills, W. Daum, C. Stuhlmann, and H. Ibach, Surf. Sci. **217**, 529 (1989).
[16]T. N. Taylor, M. A. Hoffbauer, C. J. Maggiore, and J. G. Beery, J. Vac. Sci. Technol. A **5**, 1625 (1987); T. N. Taylor, R. E. Muenchausen, M. A. Hoffbauer, A. W. Denier van der Gon, and J. F. van der Veen, *ibid.* **8**, 2732 (1990); T. N. Taylor, A. W. Denier van der Gon, and J. F. van der Veen, Phys. Rev. B **41**, 7474 (1990); T. N. Taylor, R. E. Muenchausen, and M. A. Hoffbauer, Surf. Sci. **243**, 65 (1991).
[17]E. Bauer and H. Poppa, Thin Solid Films **12**, 167 (1972).
[18]J. A. Venables, G. D. T. Spiller, and M. Handbrücken, Rep. Prog. Phys. **47**, 399 (1984).
[19]F. Gautier and D. Stoeffler, Surf. Sci. **249**, 265 (1991).
[20]E. Bauer and J. H. van der Merwe, Phys. Rev. B **33**, 3657 (1986).
[21]V. K. Kumikov and K. B. Khokonov, J. Appl. Phys. **54**, 1346 (1983).
[22]R. P. Gupta, Phys. Rev. B **23**, 6265 (1981).
[23]B. Legrand, M. Guillopé, J. S. Luo, and G. Tréglia, Vacuum **41**, 311 (1990).
[24]L. Verlet, Phys. Rev. **159**, 98 (1967).
[25]C. H. Bennett, in *Diffusion in Solids, Recent Developments,* edited by A. S. Nowick and J. J. Burton (Academic, New York, 1975), p. 73.
[26]J. Friedel, in *The Physics of Metals,* edited by J. M. Ziman (Cambridge University Press, Cambridge, 1969), p. 340.
[27]F. Ducastelle, thesis, Orsay, 1972; J. Phys. (Paris) **31**, 1055 (1970).
[28]B. Legrand and M. Guillopé in *Atomistic Simulation of Materials,* edited by V. Vitek and D. J. Srolovitz (Plenum, New York, 1989), p. 361.
[29]O. K. Andersen, O. Jepsen, and D. Glötzel, in *Highlights of Condensed Matter,* Proceedings of the International School of Physics "Enrico Fermi," LXXXIX, Varenna, Italy (North-Holland, Amsterdam, 1986).
[30]G. Allan and M. Lannoo, J. Phys. Chem. Solids **37**, 699

(1976).
[31]G. J. Ackland, M. W. Finnis, and V. Vitek, J. Phys. F **18**, L158 (1988).
[32]V. Vitek and T. Egami, Phys. Status Solidi B **144**, 145 (1987).
[33]P. C. Kelires and J. Tersoff, Phys. Rev. Lett. **63**, 1164 (1989).
[34]V. Rosato, G. Ciccoti, and V. Pontikis, Phys. Rev. B **33**, 1860 (1986).
[35]F. Ducastelle, B. Legrand, and G. Tréglia, Prog. Theor. Phys. Suppl. **101**, 159 (1990).
[36]G. Tréglia, B. Legrand, J. Eugène, B. Aufray, and F. Cabané, Phys. Rev. B **44**, 5842 (1991).
[37]C. M. Gilmore, J. A. Sprague, J. M. Eridon, and V. Provenzano, Surf. Sci. **218**, 26 (1989).
[38]J. C. Heyraud and J. J. Métois, Surf. Sci. **100**, 519 (1980).
[39]M. A. van Hove, R. J. Koestner, P. C. Stair, J. P. Biberian, L. L. Kesmodel, I. Bartos, and G. A. Somorjai, Surf. Sci. **103**, 189 (1981); **103**, 218 (1981).
[40]U. Harten, A. M. Lahee, J. P. Toennies, and C. Wöll, Phys. Rev. Lett. **54**, 2619 (1985).
[41]M. El-Batouny, S. Burdick, K. M. Martini and P. Stancioff, Phys. Rev. Lett. **58**, 2762 (1987).
[42]V. M. Hallmark, S. Chiang, J. F. Rabolt, J. D. Swalen, and R. J. Wilson, Phys. Rev. Lett. **59**, 2879 (1987).
[43]K. Takayanagi, Y. Tanishiro, K. Yagi, K. Kobayashi, and G. Honjo, Surf. Sci. **205**, 637 (1988).
[44]K. Abdelmoula and G. Nihoul, Philos. Mag. B **58**, 405 (1988).
[45]C. Wöll, S. Chiang, R. J. Wilson, and P. H. Lippel, Phys. Rev. B **39**, 7988 (1989).
[46]K. G. Huang, D. Gibbs, D. M. Zehner, A. R. Sandy, and S. G. J. Mochrie, Phys. Rev. Lett. **65**, 3313 (1990).
[47]A. Bartolini, F. Ercolessi, and E. Tosatti, in *The Structure of Surfaces II,* edited by J. F. van der Veen and M. A. van Hove, Springer Series in Surface Science Vol. 11 (Springer, Berlin, 1988), p. 132.
[48]N. Takeushi, C. T. Chan, and K. M. Ho, Phys. Rev. B **43**, 13 899 (1991).
[49]D. G. Fedak and N. A. Gjostein, Acta Metall. **15**, 827 (1967).
[50]K. H. Rieder, T. Engel, R. H. Swendsen, and M. Manninnen, Surf. Sci. **127**, 223 (1983).
[51]G. K. Binnig, H. Rohrer, C. Gerber, and E. Stoll, Surf. Sci. **144**, 321 (1984).
[52]D. Gibbs, B. M. Ocko, D. M. Zehner, and S. G. J. Mochrie, Phys. Rev. B **42**, 7330 (1990); S. G. J. Mochrie, D. M. Zehner, B. M. Ocko, and D. Gibbs, Phys. Rev. Lett. **64**, 2925 (1990); D. Gibbs, G. Grübel, D. M. Zehner, D. L. Abernathy, and S. G. J. Mochrie, *ibid.* **67**, 3117 (1991).
[53]F. Ercolessi, M. Parrinello, and E. Tosatti, Surf. Sci. **177**, 314 (1986); F. Ercolessi, E. Tosatti, and M. Parrinello, Phys. Rev. Lett. **57**, 719 (1986).
[54]B. W. Dodson, Phys. Rev. B **35**, 880 (1987).
[55]N. Takeushi, C. T. Chan, and K. M. Ho, Phys. Rev. B **43**, 14 363 (1991).
[56]M. I. Haftel (unpublished).
[57]A. D. Novaco and J. P. McTague, Phys. Rev. Lett. **38**, 1286 (1977); J. P. McTague and A. D. Novaco, Phys. Rev. B **19**, 5299 (1979).
[58]D. Wolf, H. Jagodzinski, and W. Moritz, Surf. Sci. **77**, 265 (1978).
[59]G. K. Binnig, H. Rohrer, C. Gerber, and E. Weibel, Surf. Sci. **131**, L379 (1983).
[60]I. K. Robinson, Y. Kuk, and L. C. Feldman, Phys. Rev. B **29**, 4762 (1984).
[61]G. L. Kellog, Phys. Rev. Lett. **55**, 2168 (1985).
[62]Q. Gao and T. T. Tsong, Phys. Rev. Lett. **57**, 452 (1986).
[63]T. Gustafsson, M. Copel, and P. Fenter, in *The Structure of Surfaces II,* edited by J. F. van der Veen and M. A. van Hove, Springer Series in Surface Science Vol. 11 (Springer, Berlin, 1988), p. 110.
[64]P. Fery, W. Moritz, and D. Wolf, Phys. Rev. B **38**, 7275 (1988).
[65]P. Häberle, P. Fenter, and T. Gustafsson, Phys. Rev. B **39**, 5810 (1989).
[66]M. Garofalo, E. Tosatti, and F. Ercolessi, Surf. Sci. **188**, 321 (1987).
[67]S. M. Foiles, Surf. Sci. **191**, L779 (1987).
[68]K. M. Ho and K. P. Bonnen, Europhys. Lett. **4**, 345 (1987); Phys. Rev. Lett. **59**, 1833 (1987).
[69]K. W. Jacobsen and J. F. Norskov, in *TITLE* edited by J. F. van der Veen and M. A. van Hove, Springer Series in Surface Science Vol. 11 (Springer, Berlin, 1988), p. 118.
[70]M. Guillopé and B. Legrand, Surf. Sci. **215**, 577 (1989).
[71]L. D. Roelofs, S. M. Foiles, M. S. Daw, and M. I. Baskes, Surf. Sci. **234**, 63 (1990).
[72]B. Loisel, J. Lapujoulade, and V. Pontikis, Surf. Sci. **256**, 242 (1991).
[73]B. W. Dodson, Phys. Rev. Lett. **60**, 2288 (1988).
[74]F. C. Frank and J. H. van der Merwe, Proc. R. Soc. London Ser. A **198**, 205 (1949); **198**, 216 (1949).
[75]J. H. van der Merwe, J. Microscopy **102**, 261 (1974).
[76]J. W. Matthews and A. E. Blakeslee, J. Cryst. Growth **27**, 118 (1974).
[77]J. Woltersdorf, Appl. Surf. Sci. **11/12**, 495 (1982).
[78]J. R. Willis, S. C. Jain, and R. Bullough, Philos. Mag. A **62**, 115 (1990).
[79]J. H. van der Merwe, Crit. Rev. Solid State Mater. Sci. **17**, 187 (1991).
[80]J. C. Campuzano, M. S. Foster, G. Jennings, R. F. Willis, and W. Unertl, Phys. Rev. Lett. **54**, 2684 (1985); J. C. Campuzano, A. M. Lahee, and G. Jennings, Surf. Sci. **152/153**, 68 (1985).
[81]H. Derks, J. Möller, and W. Heiland, Surf. Sci. **188**, L685 (1987).
[82]M. S. Daw and S. M. Foiles, Phys. Rev. Lett. **59**, 2756 (1987).
[83]J. Villain and I. Vilfan, Surf. Sci. **199**, 165 (1988); I. K. Robinson, E. Vlieg, and K. Kern, Phys. Rev. Lett. **63**, 2578 (1989); I. Vilfan and J. Villain, *ibid.* **65**, 1830 (1990); I. K. Robinson, E. Vlieg, and K. Kern, *ibid.* **65**, 1831 (1990).
[84]M. den Nijs, Phys. Rev. Lett. **64**, 435 (1990).
[85]D. T. Keane, P. A. Bancel, J. L. Jordan-Sweet, G. A. Held, A. Mack, and R. J. Birgeneau, Surf. Sci. **250**, 8 (1991).
[86]J. Frenkel and T. Kontorowa, Phys. Z. Sowjetunion **13**, 1 (1938).
[87]V. Rosato, M. Guillopé, and B. Legrand, Philos. Mag. A **59**, 321 (1989).
[88]C. Kittel, *Introduction to Solid State Physics* (Wiley, New York, 1976).
[89]G. Simmons and H. Wang, *Single Crystal Elastic Constants and Calculated Aggregated Properties* (MIT, Cambridge, MA, 1971).
[90]R. Hultgren, P. D. Desay, D. T. Hawkins, M. Gleiser, K. K. Kelley, and D. D. Wagman, *Selected Values of Thermodynamic Properties of the Elements* (American Society of Metals, Ohio, 1973).

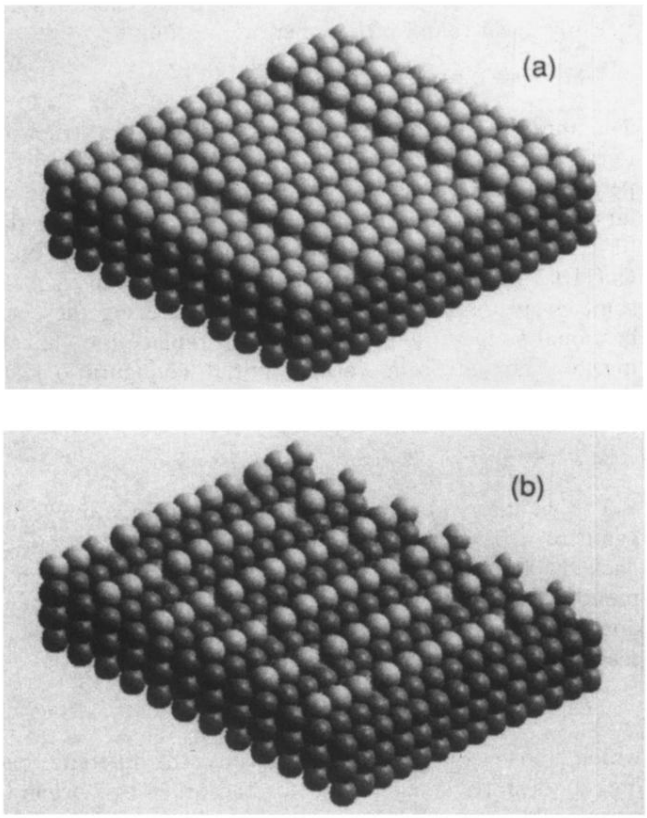

FIG. 10. Perspective view of the Ag/Cu(110) $p(1\times8)$ [(a) pseudoepitaxy, 18 unit cells] and $p(2\times7)$ [(b) missing-row reconstruction, 12 unit cells] superstructures. The white spheres indicate the Ag atoms and the black spheres indicate those of the Cu substrate.

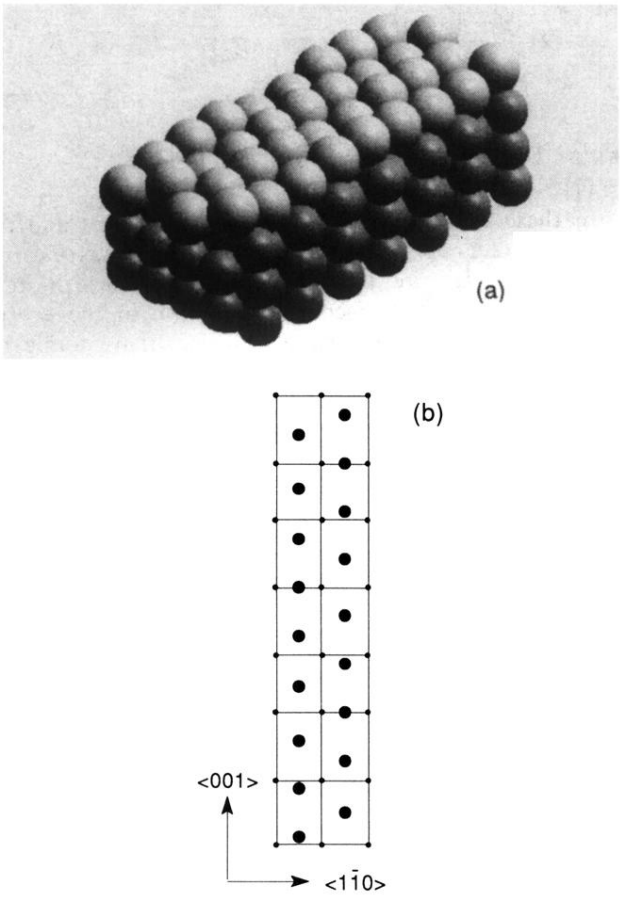

FIG. 12. $p(7\times2)$ Ag/Cu(110) pseudohexagonal structure. (a) Perspective view (two unit cells). The white spheres indicate the Ag adatoms and the black spheres indicate the Cu substrate atoms. (b) Top view (one unit cell). The large dots denote the Ag adatoms, and the small dots indicate the Cu atoms of the first underlayer.

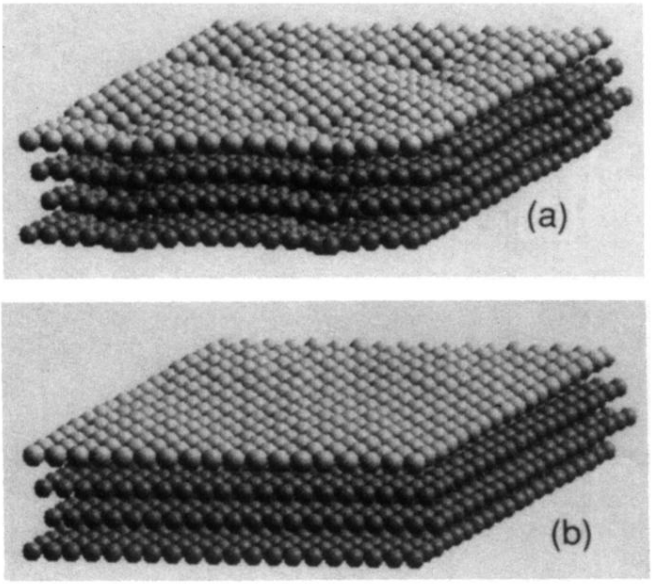

FIG. 3. Perspective view of the Ag/Cu(111) $p(10\times10)$ superstructure. Four unit cells are shown. For the sake of clarity, the scale of the z axis has been magnified by a factor of 2. The white spheres indicate the Ag atoms and the black spheres denote those of the Cu substrate: (a) fully relaxed structure (mobile substrate), (b) approximation of a rigid substrate.

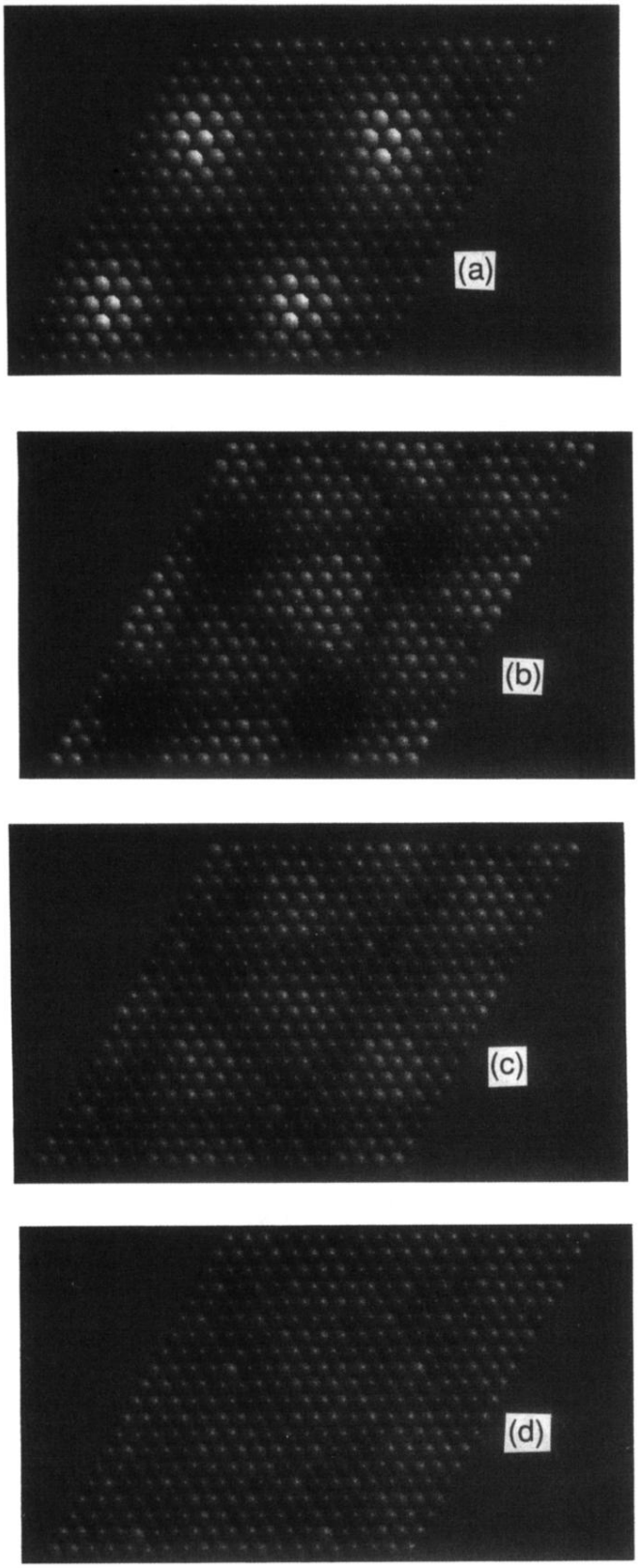

FIG. 5. Pressure map of the first four planes for the Ag/Cu(111) $p(10\times10)$ structure for the four cells shown in Fig. 3. (a) Ag adlayer, (b) Cu first underlayer, (c) Cu second underlayer, and (d) Cu third underlayer. The gray scale illustrates the pressure variation from the most tensile sites (white spheres, $P_{\min}=-135$ kbar) up to the most compressed ones (black spheres, $P_{\max}=94$ kbar).

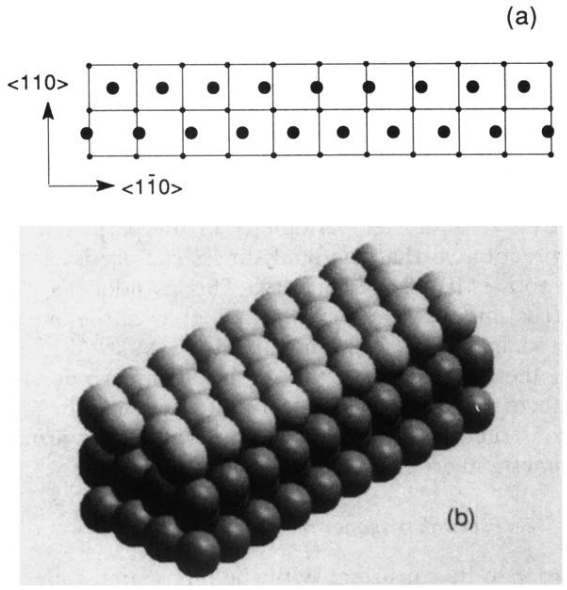

FIG. 7. $c(10\times2)$ Ag/Cu(100) pseudohexagonal structure. (a) Top view (one unit cell): the large dots denote the Ag adatoms, and the small dots denote the Cu atoms of the first underlayer. (b) Perspective view (two unit cells): the white spheres indicate the Ag adatoms and the black spheres denote the Cu substrate atoms. For the sake of clarity, the scale of the z axis has been magnified by a factor of 2.

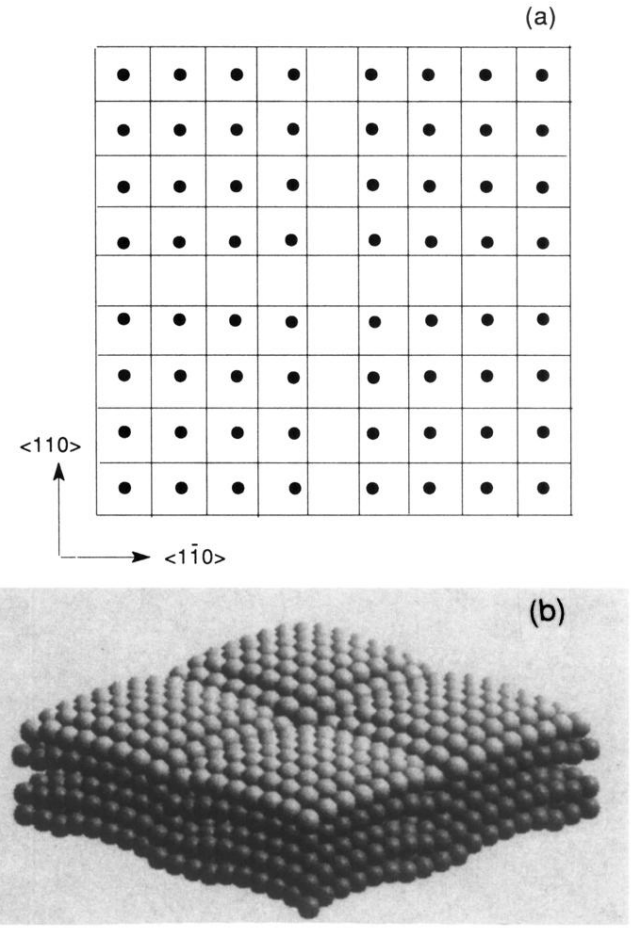

FIG. 8. $c(9\times9)$ Ag/Cu(100) pseudoepitaxial structure. (a) Top view (one unit cell): the large dots denote the Ag adatoms, and the small dots denote the Cu atoms of the first underlayer. (b) Perspective view (four unit cells): the white spheres indicate the Ag adatoms and the black spheres indicate the Cu substrate atoms. For the sake of clarity, the scale of the z axis has been magnified by a factor of 2.